New insights on the structural and optical properties of Ce–Ti mixed oxide nanoparticles doped with praseodymium

Ricardo Fernández-González, Beatriz Julián-López, Eloisa Cordoncillo and Purificación Escribano*

Received 27th May 2010, Accepted 15th September 2010
DOI: 10.1039/c0jm01625j

Nanostructured, doped Ce–Ti mixed oxides are potential materials for several applications such as pigments, catalysis, fuel cells, optical films, and gas sensors. In this article, a series of Pr-doped Ce–Ti oxides have been prepared by the solvothermal method. These compounds were characterized by XRD, Raman, N_2 sorption, SEM and UV–VIS spectrophotometry techniques. The experimental results suggest that spherical morphology, nanocrystalline particles and high specific surface area (up to 180 $m^2\ g^{-1}$) are achieved at low temperature with this free surfactant methodology. Under basic conditions, a single phase product is identified at high temperature (1000 °C), while for acid or neutral conditions, secondary phases appear. Different colored materials, ranging from yellow to red, are obtained by varying the firing temperature, quantity of doping praseodymium and the pH of the reaction. The chemical stability of these oxides was tested in some industrial polymers or glazes.

Introduction

The rational design and synthesis of advanced nanostructured materials with controllable morphology and diverse compositions has attracted tremendous interest in the field of nanoscience and nanotechnology. Since the physical and chemical properties of materials depend not only on the chemical composition but also on their porosity and shape, much effort has been focused on tailoring the pore size and external surface morphology of the materials. Some of the important applications and technologies based on nanostructured materials are: production of nanopowders of ceramics and other materials, nanocomposites, catalysts or nanoelectronics and nanodevices.

TiO_2–CeO_2 mixed oxides have attracted much interest for catalytic applications because of their improved properties. Many studies on TiO_2–CeO_2 mixtures have shown improvements regarding redox,[1,2] textural and structural properties.[3] These improvements have been attributed to modification of the structure, electronic properties, or thermal stability by Ti–Ce interaction and control of the structure. Replacing cerium ions in the CeO_2 crystalline structure (cerianite) by cations of different size or charge and which modify ion mobility inside the lattice,[4,5] results in the formation of a defective fluorite-structure.[6] Such modifications confer new properties to the material such as better resistance to sintering at high temperatures and high catalytic activity for various reactions.[7]

Scarce literature exists about the use of this mixed oxide as a matrix for luminiscent materials. The rare earth doped TiO_2–CeO_2 system offers an opportunity to study and tune the color of the material through the manipulation of energy gaps and delocalization phenomena in conduction and valence bands.[8,9] This phenomenon offers wide scope for the designing of optical materials for specific applications.

Department of Inorganic and Organic Chemistry, Universitat Jaume I, Castellón, 12071, Spain. E-mail: escriban@qio.uji.es; Fax: +0034964728214; Tel: +0034964728247

The substitution of Ce^{4+} by Pr^{4+} in pure ceria (CeO_2) systems is well-known to lead to solid solutions[10] and they produce colours ranging from brick red to dark brown, depending on the concentration of praseodymium, synthesis conditions and calcination temperatures.[11] The intense coloration of rare earth based materials arises from mostly charge transfer interactions between a donor and an acceptor with metal ions playing generally the role of an acceptor, in this case Ce^{4+} ions. In addition, the optical absorption of materials is strongly dependent on the particle size and morphology.[12] The development of preparation methods to control these parameters is needed for tapping the full potential of the mixed oxides.

As far as we know, the Pr-doped TiO_2–CeO_2 system has never been prepared using the solvothermal route, with an organic solvent like ethanol. Reddy *et al.*[13,14] obtained this solid by means of the traditional ceramic method. The conventional solid-state reaction traditionally used for the preparation of these materials involves laborious heating cycles at high temperatures with repeated grinding of the component oxides. Bondioli *et al.*[11] reported the synthesis of Pr-doped CeO_2 by a microwave-assisted hydrothermal route, reducing the reaction time under pressured conditions. Crystalline nanoparticles of ~30 nm in diameter and specific surface areas ranging from 28 to 37 $m^2\ g^{-1}$ were obtained.

The present paper is focused on the production of nanostructured Pr-doped TiO_2–CeO_2 powders by a simple solvothermal methodology. We are able to synthesize nanocrystalline products at moderate temperature (170 °C) with a good control over particle shape and high specific surface area (~180 $m^2\ g^{-1}$). Synthetic parameters have been modified in order to get materials with a single phase. These features are especially interesting for reducing energetic costs, for stabilizing the dispersion required in ceramic ink technologies and reliable jet operations of the print head. Also it is important because it reduces the quantity of the rare-earth precursors, which are expensive. Our study addresses the synthesis, characterization and applications. The results provide new insights on the influence of composition and synthetic parameters such as pH,

complexing agent, precursors, *etc.* on the characteristics of Pr doped TiO_2–CeO_2 mixed oxide such as their nanocrystallite structure, crystallite size, pore structure, surface area, and optical properties.

Experimental methods

Synthesis

Several samples with the stoichiometry $Ce_{0.5-x}Pr_xTi_{0.5}O_2$ ($x = 0$, 0.025, 0.05, 0.1, 0.5) were prepared by a solvothermal methodology. The general synthesis protocol described herein corresponds to the production of 2 g of the final mixed oxide. The stoichiometric amounts of the cerium and praseodymium precursors ($Ce(NO_3)_6(NH_4)_2$, 98.5%, and $Pr(NO_3)_3$, 99.9%, both from Strem Chemicals) were dissolved in 60 mL of ethanol according to Scheme 1. Acetylacetone (acac) was mixed with tetraisopropyl orthotitanate (Fluka Chemika), and then added to the Ce–Pr solution. The solution was stirred for 30 min and transferred into the Teflon cup of a 125 mL Parr acid digestion bomb. The solvothermal treatment was conducted at 170 °C for 4 days. A brown precipitate was obtained as the reaction product which was washed with ethanol and dried in air. The dried product was calcined in air at different temperatures from 500 °C to 1000 °C and held at each temperature for 2 h. The synthesis procedure was repeated several times in order to prove the reproducibility.

The metal : acac molar ratio was varied (1 : 1, 1 : 2 and 1 : 4) in order to study the role of the complexing agent on the synthesis mechanism. The reaction pH was also modified by adding acid (acetic acid, pH = 4) and basic (NaOH, pH = 12) solutions before introducing the mixture into the Teflon cup in order to investigate the influence of acid and base as catalysts on the hydrolysis and condensation reactions.

Characterization

Phase analyses of the calcined powders were characterized by X-ray powder diffraction (XRD) with a SIEMENS D5000. The patterns were collected in the range of $2\theta = 15$–$70°$ with a step scan of 0.05° and 1.5 s counting time at each step. The goniometer was controlled by the "SIEMENS DIFFRACT plus" software. Laser Raman spectra were recorded on a Raman Jasco NRS-3100 spectrometer equipped with a confocal microscope and a CCD detector air-cooled to −65 °C. The sample excitation and Raman scatter collection were performed using a 532 nm excitation line, 100× optical lens, with 5 s exposure time and 25 scans. N_2 Adsorption–desorption isotherms were collected on a Micromeritics Gemini V gas adsorption analyzer at 77 K, after degassing the samples at 423 K overnight in a Micromeritics Flow prep 060 system with nitrogen flux gas. The BET surface areas were calculated from the adsorption branch of the isotherm by the BJH method. UV/Vis/NIR spectroscopy and the colorimetric study of the samples were carried out with a CARY 500 SCAN VARIAN spectrophotometer in the 300–800 nm range. The diffuse reflectance spectra (DRS) were obtained by using an integrating sphere and $BaSO_4$ as reference. The CIELAB colour parameters L* a* b* were determined by coupling an analytical software for colour measurements to the VARIAN spectrophotometer. In the CIELAB system, L* is the lightness axis [black (0) to white (100)], a* is the green (<0) to red (>0) and b* is the blue (<0) to yellow (>0) axis. Scanning electron micrographs of the samples were taken with a field emission gun scanning electron microscope (FEG-SEM) model JEOL 7001F, equipped with a spectrometer of energy dispersion of X-ray (EDX) from Oxford instruments by using the following operational parameters: acceleration voltage 20 kV, measuring time 100 s, working distance 25 mm, counting rate 1.2 kcps.

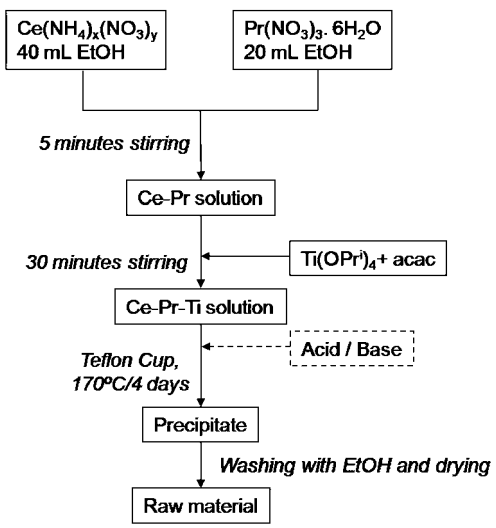

Scheme 1 General scheme of the solvothermal synthesis

Applications

The chemical stability of the obtained colored materials was evaluated in polymers and glazes for ceramic tiles.

With the yellow material fired at low temperature (500 °C), 3% and 8% in weight of the pigment was mixed with low density polyethylene (LDPE). The polymer blends were obtained by melt blending in an internal mixer (Haake Polylab) during a mixing time of 5 min at a temperature of 150 °C. The mixing was performed at a rotor speed of 60 rpm. The batch was extracted from the mixing chamber manually and allowed to cool to room temperature in air. The mixed polymer was finally transformed into sheets (0.8 mm thick) by compression molding in a hot-plate hydraulic press at 125 °C and 2 MPa of pressure during 4 min. The intensity of the color of the plastics depends on the concentration of the pigments.

The application of the red material fired at 1000 °C as a pigment for glazes was conducted as follows: 4% in weight of the pigment was mixed with an industrial glaze, using water as a dispersing medium, and applied to white twice-fire bodies. After drying, the pieces were fired in an electric, conventional kiln, following an industrial, low temperature firing cycle where the highest temperature of the cycle was 750 °C for 10 min.

Results and discussion

Compositional study

A preliminary study modifying the Ce/Pr and Ce/Ti molar ratio from the general $(Ce,Pr)_{0.5}Ti_{0.5}O_2$ composition was performed.

Table 1 Crystalline phases (detected by XRD) and CIELAB chromatic coordinates of the prepared Ce–Pr–Ti oxide compositions. C = CeO_2 (cerianite), R = TiO_2 (rutile), *A* = TiO_2 (anatase) (JCPDS No. 21–1272), CT = $CeTi_2O_6$, P = Pr_6O_{11} (JCPDS No. 42–1121), PT = $Pr_2Ti_2O_7$ (JCPDS No. 35–267).

	Crystalline phases at 500 °C	Crystalline phases at 1000 °C	CIELAB chromatic coordinates at 500 °C			CIELAB chromatic coordinates at 1000 °C		
			L*	a*	b*	L*	a*	b*
$Ce_{0.1}Pr_{0.1}Ti_{0.8}O_2$	A	C + R + CT	61 84	10 98	21 13	78 86	10 60	19 25
$Ce_{0.4}Pr_{0.1}Ti_{0.5}O_2$	C	C + R + CT	57 78	12 96	40 81	60 30	23 07	25 66
$Ce_{0.6}Pr_{0.1}Ti_{0.3}O_2$	C	C + R + CT	93 26	−3 35	34 40	59 33	15 86	17 32
$Ce_{0.5}Ti_{0.5}O_2$	C	C + CT	80 57	4,10	35 64	96 25	−3 09	24 84
$Ce_{0.475}Pr_{0.025}Ti_{0.5}O_2$	C	C + R + CT	73 44	11 02	54 99	64 84	21 58	24 71
$Ce_{0.45}Pr_{0.05}Ti_{0.5}O_2$	C	C + R + CT	62 29	14 19	47 34	60 61	23 78	26 33
$Ce_{0.4}Pr_{0.1}Ti_{0.5}O_2$	C	C + R + CT	57 78	12 96	40 81	60 30	23 07	25 66
$Pr_{0.5}Ti_{0.5}O_2$	P + PT	P + PT	58 78	12 96	40 82	69 17	−0 73	1 67

Table 1 summarizes crystalline phases and chromatic coordinates of a series of Pr-doped Ce–Ti oxides that were prepared according to the standard solvothermal route described in the experimental section (with a 1 : 2 metal : acac molar ratio and without adding any acid or basic solution). At 500 °C, DRX patterns suggest a low cristalline structure, however it is possible to assign the broad peaks to the phases mentioned in Table 1. After calcination at 1000 °C, no single crystalline phase was obtained, indicating that the synthesis conditions were not optimized. Therefore, a more detailed study is discussed in the next section.

Despite these conclusions, an important achievement was that the color of the materials ranged from yellow to red-brown depending on the Ce/Pr/Ti content and the temperature. For the series with a praseodymium constant ratio, intense yellow (high b*) and red (high a*) colorations were achieved for the $Ce_{0.4}Pr_{0.1}Ti_{0.5}O_2$ sample. An extensive study of a similar composition, $Ce_{0.45}Pr_{0.05}Ti_{0.5}O_2$, allowed the detection of similar chromatic coordinates. Therefore this stoichiometry was selected in order to optimize synthesis conditions and improve the reactivity and the homogeneity of the system.

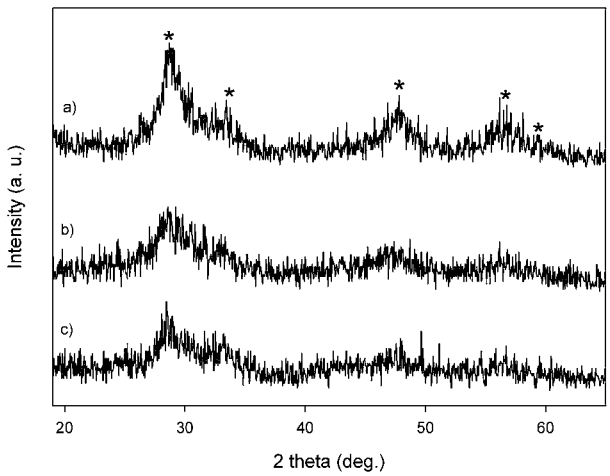

Fig. 1 XRD patterns of the raw samples prepared under basic conditions with different M : acac ratio: a) M : acac ratio 1 : 1, b) M : acac ratio 1 : 2, c) M : acac ratio 1 : 4.

Study of synthesis conditions: complexing agent

X-ray diffraction patterns of the as-synthesized $Ce_{0.45}Pr_{0.05}Ti_{0.5}O_2$ sample prepared with different metal : acac ratios under basic conditions are shown in Fig. 1. It is important to mention that, in other conditions, amorphous powders were obtained (not shown) and no conclusions can be extracted. This behaviour is in agreement with other studies, in which it has been demonstrated that the pH of the synthesis strongly affects the morphology[15] and crystallinity[16] of nanomaterials prepared by solvothermal routes.

The XRD profiles of the powders obtained after solvothermal treatment of the precursor solution at 170 °C under basic conditions show some weak and broad diffraction peaks that can be attributed to the presence of nanocrystalline cubic CeO_2 (cerianite, JCPDS No. 34–394), the positions of which are marked in Fig. 1 with asterisks.

Since the radii of Ti^{4+} ions in eightfold coordination is 0.88 Å, it can occupy the Ce coordination sites in the cubic ceria structure (radius of Ce^{4+} is 1.11 Å). This behaviour has already been reported by Fang *et al.*[17] They propose a reaction mechanism for TiO_2–CeO_2 mixed oxides based on the formation of a Ti–CeO_2 solid solution at low temperature. Our XRD patterns (Fig. 1) do not show signals corresponding to crystalline titanium species, which could be in agreement with the results obtained by Fang *et al.* However, existence of amorphous TiO_2 can not be discarded.

The highest crystallinity is exhibited by the sample with 1 : 1 metal : acac ratio (Fig. 1a), and the XRD patterns are less

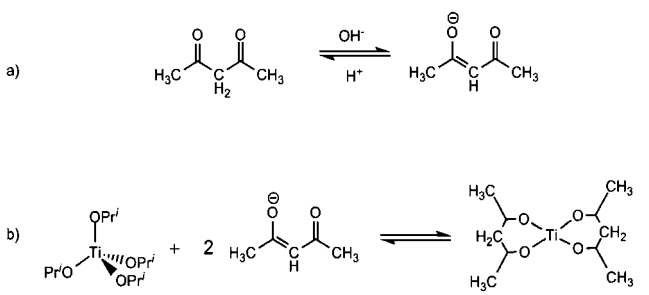

Scheme 2 a) Keto–enolic equilibrium of acetylacetone; b) complexation of monomeric Ti precursor in presence of acac molecules.

defined for the other two samples (lower crystallinity). This behaviour can be explained through the competitive growth/termination mechanism of metal-oxo species in the presence of acac surface capping agents. According to our synthesis procedure, the $Ti(OPr^i)_4$ precursor, which appears as a monomeric specie[18] is firstly mixed with acetylacetone and, in the absence of any solvent, the complexation of Ti ions by the chelating agent occurs. According to Scheme 2, a 1 : 1 metal : acac (equivalent to 1 : 2 Ti : acac) ratio could satisfy all the coordination positions of the Ti metal by coordination expansion. Obviously, for higher acac amounts, an excess of complexing agent is present in the medium.

In the next synthetic step, where the Ti–acac mixture is added to the ethanolic Ce–Pr solution, a color change (from brown to pale yellow) is observed. It means that a complexation of the cerium and praseodymium ions with the acac agent has occurred. A colloidal precipitate appears when the basic solution is added. This precipitation is a consequence of the important increase of the hydrolysis and condensation rates that take place by an S_N2 mechanism, even if the keto–enolic equilibrium of the acac (Scheme 2) is shifted towards the coordinating enol form. That is the reason why the solids obtained after solvothermal treatment already exhibit some crystallinity by XRD.

Under neutral or acid conditions, the effectiveness of the complexing agent (Scheme 2) is not so high which is demonstrated by the limited metal–acac complexation reaction. Since the M–acac bonds remain stable upon hydrolysis reactions, such chelating ligands play a key role. Furthermore, the low pH increases the hydrolysis ratio but limits the condensation of the M–OH groups. Both factors, catalysis and capping ligands, control the spatial extension of the oxide core and the functionality of the precursors. All these parameters result in a higher crystalline ceria under low acac concentration and basic conditions.

Recent investigations into the sol–gel formation mechanisms of solids,[19] point out that that nanosized mixed oxides are obtained from heterometallic oligomers. In our system, Ti–Ce–Pr oxo-oligomers would be formed during solvothermal treatment and their size and shape would be controlled by the acac content. Therefore, a decisive factor in formation of the heterometallic complexes is the choice of the ligands with proper composition and sterical requirements to be able to provide the right number of donor functions and the protection of the chosen core of metal and donor atoms.[20] So, the 1 : 2 metal : acac ratio was chosen as a standard for the next acid-basic study at higher temperatures.

Study of synthesis conditions: pH medium

X-ray diffraction patterns of the $Ce_{0.45}Pr_{0.05}Ti_{0.5}O_2$ sample prepared at different pH conditions, after calcination at 500 °C, are shown in Fig. 2.

At this temperature, the XRD profiles show the broad diffraction peaks corresponding to the nanocrystalline cerianite structure. No peaks assigned to TiO_2 crystalline phases are detected. It can be observed that both acid and basic addition in the synthesis help the crystallization of the system. In the case of acid addition, this result can be explained by the increasing hydrolysis rate induced by the protonation of the alkoxy ligands

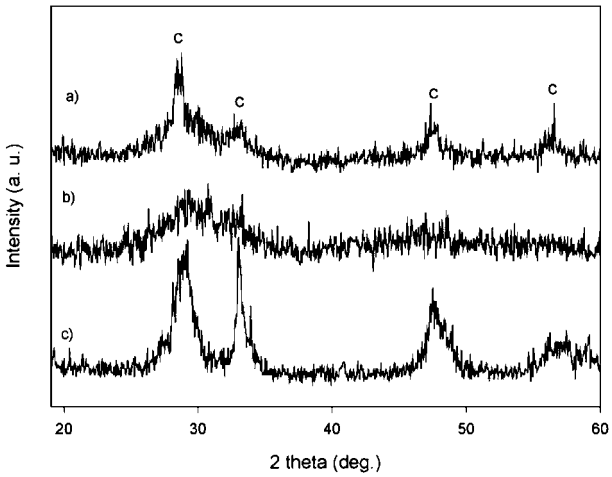

Fig. 2 XRD patterns of the $Ce_{0.45}Pr_{0.05}Ti_{0.5}O_2$ sample prepared with 1 : 2 metal : acac ratio at different pH conditions by adding: a) acetic acid, b) no addition, c) NaOH, after heat treatment at 500 °C for 2 h. C = CeO_2 (cerianite).

which therefore become better leaving groups. The effect of the base addition has already been explained in Fig. 1. A shift towards higher 2θ is clearly detected when basic solution is added, indicating that Ti^{4+} ions enter into the CeO_2 network. This point reveals a good control of the complexing agent (enol-form) on the hydrolysis and condensation rates of both Ce and Ti precursors, leading to CeTi heterometallic oligomers. In contrast, this shift is not observed in the other samples. Given that praseodymium oxide presents, as does CeO_2, a fluorite structure and also that Ce^{4+} and Pr^{4+} have similar ionic radii, these two oxides form solid solutions in a wide range of compositions, and no shift of the XRD peaks could be noted.[10]

The average crystallite size of the samples was estimated using the Scherrer equation from the full-width at half maximum (FWHM) of the most intense peak, after correction by the instrumental line broadening. The crystalline domain size, assuming spherical morphology, was estimated to be between 4 and 7 nm.

Fig. 3 shows the XRD diffractograms of the samples prepared in different pH media after firing at 1000 °C.

The patterns reveal that only under basic conditions (Fig. 3d), cubic CeO_2 is obtained as a single phase. A shift towards higher 2θ values on the peak position agrees with the incorporation of Ti ions into the fluorite network, leading to a solid solution, as already reported.[17] For the other samples, new peaks associated with secondary phases are visible. They can be assigned to rutile (TiO_2, JCPDS No.21–1276) and $CeTi_2O_6$.[21–24] Some controversy exists about the last phase, which is not included on the JCPDS list, but according to several authors it corresponds to a brannerite-based structure in which Ce^{4+} would be in in octahedral coordination. This coordination is quite unusual for this rare earth ion and its stability is still questioned.

Quantitative analysis of the different phases could be performed to deeply delve into this question but this point is beyond the scope of the present study.

Taking into account that a single phase is demanded for specific applications, basic conditions are essential to achieve ceria solid solutions at high temperature.

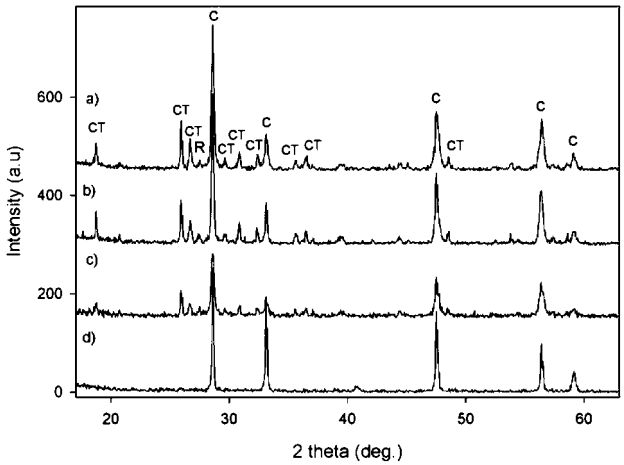

Fig. 3 XRD patterns of the $Ce_{0.45}Pr_{0.05}Ti_{0.5}O_2$ sample prepared with 1 : 2 metal : acac ratio at different pH conditions by adding: a) nitric acid, b) acetic acid, c) no addition, d) NaOH, after heat treatment at 1000 °C for 2 h. C = CeO_2 (cerianite), R = TiO_2 (rutile), CT = $CeTi_2O_6$.

It is well-known that acetic acid can behave as a ligand and bond to metal of alkoxide metals in a bidentate or bridging way. The presence of this ligand could affect the keto–enolic equilibrium of acac and modify the reactivity of the system. In order to be sure that the development of secondary phases is related to the acid media and not to the possible complexation by acetate ions, the synthesis was also performed using nitric acid as catalyst. The experiment led to the same results: rutile and $CeTi_2O_6$ as secondary phases (Fig. 3a and 3b).

At this temperature, the average crystallite size calculated from the Scherrer equation of the most intense CeO_2 peak was estimated to be around 35 nm and 65 nm for acid/neutral and basic conditions, respectively.

In order to assess the structural features, particularly about the unusual $CeTi_2O_6$ phase, laser-Raman spectroscopy experiments were carried out. The spectra for the representative sample fired at 1000 °C are depicted in Fig. 4.

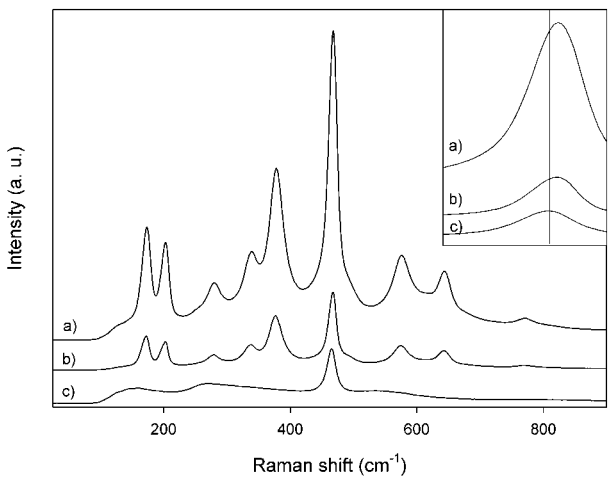

Fig. 4 Raman spectra of the $Ce_{0.45}Pr_{0.05}Ti_{0.5}O_2$ sample prepared with 1 : 2 metal : acac ratio at different pH conditions by adding: a) no addition, b) acetic acid, c) NaOH, after heat treatment at 1000 °C for 2 h. Inset: detail of the first order CeO_2 peak at around 465 cm^{-1}.

The sharp band located at 465 cm^{-1} that appears in all the spectra is assigned to the symmetric vibration of CeO_2[25,26] (space group: *Fm3m*). The peak position of this strong, triply degenerate, first order Raman line is shifted to lower energies in the basic sample (see inset of Fig. 4). This is in agreement with a smaller lattice parameter[27,28] as a consequence of the Ti^{4+} incorporation inside the CeO_2 network. In non-basic samples, the Raman measurements suggest that Ce cations are replaced by Pr ions instead of smaller Ti cations. This point is also corroborated by optical properties (red color) and related to a crystal field effect on the efficiently Pr-doped mixed oxide. Furthermore, in non-basic samples, a set of bands at 164, 197, 278, 335, 376, 576 and 644 cm^{-1} are found. According to Fu *et al.*[29] they can be attributed to the Raman-active modes of the $CeTi_2O_6$ structure. No signal corresponding to the rutile phase, expected at 610 cm^{-1}, has been detected by Raman spectroscopy.

The morphology and dimensions of the Ce–Pr–Ti oxide particles have been studied by scanning electron microscopy (SEM). Fig. 5 illustrates two representative examples of the $Ce_{0.45}Pr_{0.05}Ti_{0.5}O_2$ composition, since there are no significant differences with the thermal treatment.

A general view of the materials reveals that the particles exhibit spherical morphology with a size distribution ranging from 200 nm to 3 μm. This morphology is usually achieved for synthetic treatments where the precursors are modified with chelating organic ligands. The chelation controls the hydrolysis and condensation processes, and helps the stabilization of the heterometallic nanocrystals in organic solvents. Indeed, the hydrophobic β-diketonate acts as a capping agent covering the surface of the oxide colloids.[30,31]

Thermal treatment at higher temperatures induces decomposition of organic compounds anchored at the surface, and the nanospheres agglomerate leading to larger particles.

The spherical morphology of the particles can be attributed to the organic surface modification of the inorganic oxidic nuclei during solvothermal treatment. The organic modification also

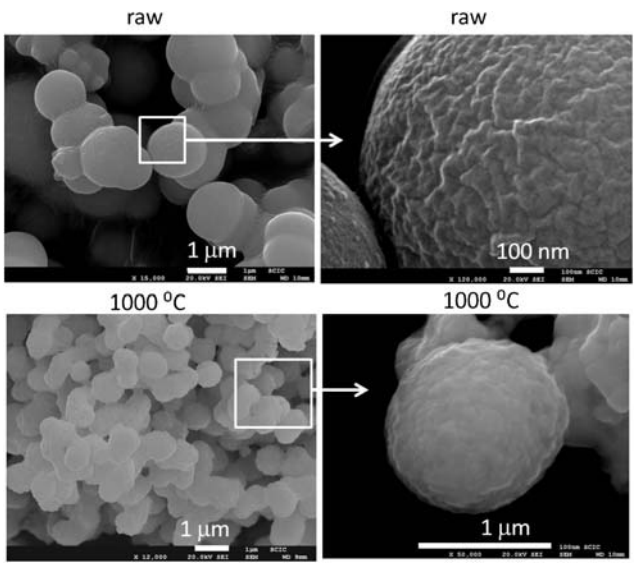

Fig. 5 Scanning electron micrographs of the as-synthesized (raw) $Ce_{0.45}Pr_{0.05}Ti_{0.5}O_2$ sample and after firing at 1000 °C.

allows nanospheres to be dispersed. This morphology is of interest for novel technologies employing suspensions because it opens the field to new applications for catalysis,[32–34] fuel cells,[35–37] optical films,[38] polishing materials, gas sensors[39,40,41,42] and pigments.[43,44]

It is also remarkable to note that the spheres exhibit a rough surface (Fig. 5), indicating the existence of an external open porosity. The chemical composition of the different samples was conducted by energy-dispersive X-ray spectroscopy. The surface analysis indicated that the samples were not completely homogeneous, as expected from XRD and Raman measurements.

N_2 Adsorption–desorption isotherms plots of the sample fired at different temperatures are shown in Fig. 6.

The curves can be associated with reversible type IV adsorption–desorption isotherms with a small H2 type hysteresis loop at 170 °C and 500 °C. These kind of curves are usually related to mesoporous materials with pore diameter smaller than 4 nm, where pores are completely filled and emptied at similar pressures, resulting in a reversible adsorption–desorption isotherm.

The raw sample obtained after solvothermal treatment for four days at 170 °C exhibits a high value of specific surface area, S_{BET} up to 182.30 $m^2\ g^{-1}$. In spite of the fact that this sample still contains organic matter, such a high surface area must be associated with internal porosity inside the microspheres. This structure of the material could be responsible for the roughness of the external surface of the microspheres, previously noted by SEM techniques. An increase on the firing temperature results in a diminution of the BET surface area (S_{BET} up to 1.51 $m^2\ g^{-1}$ at 1000 °C), as a consequence of crystalline growth and sinterization processes. However, high values are still obtained at elevated temperatures, for instance, 38 $m^2\ g^{-1}$ have been measured after heat treatment at 500 °C.

The high surface area of our materials is of great interest for catalysis, since the catalytic reactions take place on the surface of the solids. The solvothermal route, proposed in this work as a general synthetic route for mixed metal oxides, provides porosity generated *in situ* during the treatment from decomposition of organic moieties (acetylacetone groups).

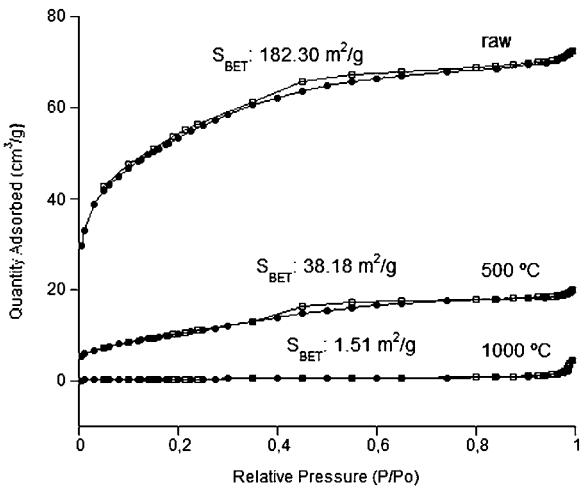

Fig. 6 Nitrogen adsorption–desorption isotherms of the $Ce_{0.45}Pr_{0.05}Ti_{0.5}O_2$ sample fired at the indicated temperatures. The values of specific surface area (S_{BET}) calculated from the desorption branch of the isotherm using the BJH method.

Optical study

Fig. 7 presents UV/VIS absorption spectra of the prepared samples under different pH conditions. The method of UV/VIS diffuse reflectance spectroscopy was employed to estimate band-gap energies (E_g) of the prepared samples. Firstly, to establish the type of band-to-band transition in these synthesized particles, the absorption data were fitted to equations for direct band-gap transitions. The E_g value was estimated from the inflexion point of the curves.

The curve of the sample prepared with basic solution is dominated by an absorption band located below 450 nm. The fitting of the spectrum proportioned a band gap value of 460 nm (2.70 eV), associated with the characteristic charge transfer between the O^{2-} valence and the Ce^{4+} conduction bands.[45] This band is red-shifted (~50 nm) in comparison to pure CeO_2–TiO_2 materials already prepared in our group.[46] This effect can be attributed to a small substitution of Ce^{4+} ions by Pr^{4+} ions,[47] but also to the different preparation methods and particle sizes.

In the UV/VIS spectra of the other samples, this absorption is shifted towards the visible region. The band gap is now around 597 nm (2.07 eV). The red-shift is a consequence of the introduction of additional energy levels ($4f^1$ electrons) from the praseodymium ion which, under these conditions, is more efficiently incorporated into the CeO_2 network than in the basic ones. In addition, the presence of a secondary phase ($CeTi_2O_6$) provides a different coordination site for Ce/Pr ions that can modify the absorption properties; due to a low coordination number (6 instead of 8) and a change in the crystalline field.

In Table 2, the CIEL*a*b* chromatic coordinates of these samples after calcination at 500 °C and 1000 °C are presented.

At 500 °C, a yellow coloration (high b* chromatic coordinate) is detected after Pr-doping but a more pale shade is achieved when basic conditions are applied. The coefficient h_{ab} (hue angle) close to the 90° expected for an ideal yellow color, confirms the visual observations.[48]

At 1000 °C, it is clear from Table 2 that doping the system Ce–Ti with praseodymium drastically increases the red component (a*) from −3.09 to 25.15, which is in agreement with the features of the UV/VIS absorption spectra. There is no change in the

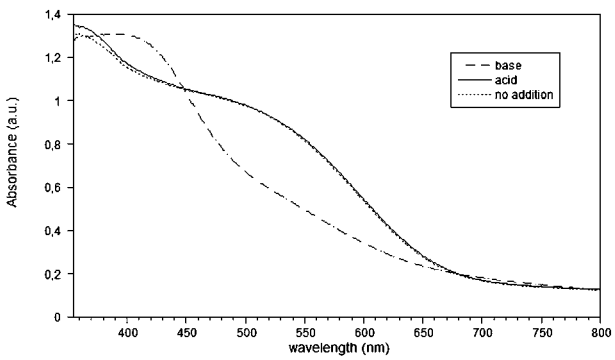

Fig. 7 UV/VIS spectra of $Ce_{0.45}Pr_{0.05}Ti_{0.5}O_2$ sample at different pH conditions after heat treatment at 1000 °C for 2 h.

Table 2 CIELAB chromatic coordinates of the powder samples: $Ce_{0.5}Ti_{0.5}O_2$ as reference, $Ce_{0.45}Pr_{0.05}Ti_{0.5}O_2$ under different pH conditions and test pieces of LPDE plastic (with 3% and 8% in weight of pigment) and ceramic glaze (with 4% in weight of pigment)

	500 °C					1000 °C		
Sample	L*	a*	b*	C_{ab} [a]	h_{ab} [b]	L*	a*	b*
$Ce_{0.5}Ti_{0.5}O_2$	80.57	4.1	35.64	35.88	83.43	96.25	−3.09	24.84
Acid	62.61	13.4	46.02	47.93	73.76	51.12	25.15	26.13
No addition	62.29	14.19	47.34	49.42	73.31	50.59	24.78	25.26
Basic	71.06	7.91	43.23	43.95	79.60	53.69	8.55	37.68
3% wt-LDPE	65.5	−1.69	34.92	34.96	87.22	—	—	—
8% wt-LDPE	58.23	3.68	40.89	41.06	84.85	—	—	—
4% wt-Glaze	—	—	—	—	—	52.72	23.68	25.4

[a] $C_{ab} = \sqrt{a^2 + b^2}$: purity of hue (0–100). [b] h_{ab} = arctan (a/b): angle of hue (yellow = 90°).

yellow component (b*). In contrast, for basic conditions brownish color is obtained.

The chemical and thermal stability, as well as the coloring performance of the materials were tested for polymers and ceramic glazes (Fig. 8). Good results were achieved for both applications.

The incorporation of different percentages of the colored materials provided an homogeneous yellow shade in the polyethylene plastic. The small size and the spherical morphology of the powders permit a high dispersion inside the LDPE plastic. As expected, the b* coordinate (yellow component) depended on the concentration of the pigment. Gauthier *et al.*[48] provided a similar yellow cerium compound for applications in plastics with a low thermal stability. Taking into account that industrial processes usually require high temperatures, cerium thiosilicates (Ce–S–Si phases) can decompose leading to hazardous SO_2 and losing their properties. Our results represent a significant improvement in terms of thermal and chemical stability.

In more aggressive media such as ceramic glazes, the powders resulted to be chemically stable. The CIELAB chromatic coordinates (Table 2) of powders and glazed tiles were similar. As we saw before a good homogeneity on the coloration due to a high dispersion provided by the morphology and small size of the particles was obtained.

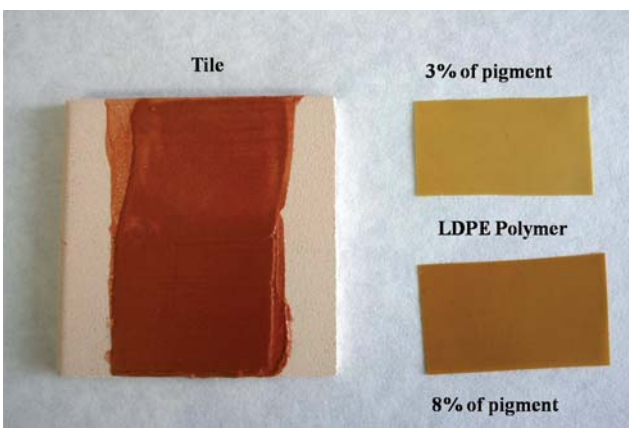

Fig. 8 Picture showing the chemical stability of the yellow and red materials ($Ce_{0.45}Pr_{0.05}Ti_{0.5}O_2$ fired at 500 °C and 1000 °C) in a LDPE polymer and a ceramic glaze, respectively.

Conclusions

Pr-Doped cerium-titanium mixed oxides were prepared by an easy solvothermal method that allows a good control over particle size, shape, crystallinity and surface properties. Different synthetic conditions such as metal/acetylacetone molar ratio and pH of the reaction medium were tested. The structural characterization performed by XRD reveal the crystalline nature of the materials at low temperature, and a change in the crystalline phases depending on the pH. An interesting CeO_2 single phase is obtained upon basic conditions; meanwhile secondary phases (TiO_2 and $CeTi_2O_6$) are developed in other conditions. The presence of these phases has been corroborated by Raman spectroscopy. Scanning electron microscopy provided excellent pictures illustrating the spherical shape and bumpy texture in the materials, even at 1000 °C. N_2 Sorption demonstrated that we have porous materials with high specific surface area after solvothermal treatment. UV/VIS measurements, including absorption spectra and CIELAB chromatic coordinates, allowed us to understand the optical properties of the samples, specifically the yellow and red colorations. In addition, it was found that Pr cations, responsible for red coloration,[10,11] were more efficiently incorporated into the CeO_2 network under acid conditions. The chemical stability of these oxides was tested in some industrial polymers or glazes. In conclusion, the present analysis contributes to the detailed elucidation of the structural, optical and chemical properties of Pr-doped nanostructured ceria-titania mixed oxides that may find direct applications in ceramic ink-jet technologies and polymer pigments.

Acknowledgements

This research was supported by the Spanish Government and MAT (2008-03479) and Bancaixa Foundation—Universitat Jaume I (P1 1B2007-47) projects. B.J.-L. is especially thankful to MEC for "Ramón y Cajal Program" contract. Dr L. Cabedo is grateful acknowledged for his help in the preparation of the polymers.

Notes and references

1 G. W. Koebrugge, L. Winnubst and A. J. Burggraaf, *J. Mater. Chem.*, 1993, **3**, 1095.
2 Z. M. Shi, W. G. Yu and X. Bayar, *Scr. Mater.*, 2004, **50**, 885.
3 T. Lopez, F. Rojas, R. Alexander-Katz, F. Galindo, V. Balankin and A. Buljan, *J. Solid State Chem.*, 2004, **177**, 1873.
4 B. K. Cho, *J. Catal.*, 1991, **131**, 74.
5 M. O. Connell and M. A. Morris, *Catal. Today*, 2000, **59**, 387–393.
6 J. Rynkowski, J. Farbotko, R. Touroude and L. Hilaire, *Appl. Catal., A*, 2000, **203**, 335.
7 M. Pijolat, M. Prin, M. Soustelle, O. Tourer and P. J. Nortier, *J. Chem. Soc., Faraday Trans.*, 1995, **91**, 3941.
8 L. S. Kumari, G. George, P. P. Rao and M. L. P. Reddy, *Dyes Pigm.*, 2008, **77**, 427.
9 P. P. Rao and M. L. P. Reddy, *Dyes Pigm.*, 2007, **73**, 292.
10 H. Borchert, Y. V. Frolova, V. V. Kaichev, I. P. Prosvirin, G. M. Alikina, A. I. Lukashevich, V. I. Zaikovskii, E. M. Moroz, S. N. Trukhan, V. P. Ivanov, E. A. Paukshtis, V. I. Bukhtyarov and V. A. Sadykov, *J. Phys. Chem. B*, 2005, **109**, 5728.
11 F. Bondioli, A. M. Ferrari, L. Lusvarghi, T. Manfredini, S. Nannarone and V. Pasquali, *J. Mater. Chem.*, 2005, **15**, 1061.
12 *Industrial inorganic pigments*, ed. G. Buxbaum, VCH: Weinheim, Germany, 1993.
13 L. S. Kumari, G. George, P. P. Raom and M. L. P. Reddy, *Dyes Pigm.*, 2008, **77**, 427.
14 G. George, P. P. Rao and M. L. P. Reddy, *Chem. Lett.*, 2006, **35**, 1412.
15 T. J. Boyle, T. N. Lambert, H. D. Pratt III, P. Lu, J. J. M. Griego, N. Bush, C. A. Chavez and M. Welk, *J. Mater. Sci.*, 2010, **45**, 1744.
16 A. M. T. Silva, B. F. Machado, H. T. Gomes, J. L. Figueiredo, G. Drazic and J. L. Faria, *J. Nanopart. Res.*, 2010, **12**, 121.
17 J. Fang, X. Bi, D. Si, Z. Jiang and W. Huang, *Appl. Surf. Sci.*, 2007, **253**, 8952.
18 *Sol–Gel Science: The Phsysics and Chemistry of Sol–Gel*, ed. J. C. Brinker and G. W. Scherrer, Processing: Academic Press, San Diego, 1990.
19 V. G. Kessler, *J. Sol-Gel Sci. Technol.*, 2009, **51**, 264–27.
20 V. G. Kessler, *Chem. Commun.*, 2003, 1213.
21 M. Fu, L. Wei, Y. Li, S. Hao and Y. Li, *Solid State Sci.*, 2009, **11**, 2133.
22 T. Kidchob, L. Malfatti, D. Marongiu, S. Enzo and P. Innocenzi, *Thin Solid Films*, 2010, **518**, 1653.
23 X. Jiang, L. Lou, Y. Chen and X. Zheng, *Catal. Lett.*, 2004, **94**, 49.
24 J. Rynkowski, J. Farbotko, R. Touroude and L. Hilaire, *Appl. Catal., A*, 2000, **203**, 335.
25 J. E. Spanier, R. D. Robinson, F. Zang, S. W. Chan and I. P. Herman, *Phys. Rev. B: Condens. Matter*, 2001, **6424**, 2454071.
26 W. H. Weber, K. C. Hass and J. R. McBride, *Phys. Rev. B: Condens. Matter*, 1993, **48**, 178.
27 J. E. Spanier, R. D. Robinson, F. Zhang, S.-W. Chan and I. P. Herman, *Phys. Rev. B: Condens. Matter Mater. Phys.*, 2001, **64**, 245407.
28 J. R. McBride, K. C. Hass, B. D. Poindexter and W. H. Weber, *J. Appl. Phys.*, 1994, **76**, 2435.
29 M. Fu, L. Wei, Y. Li, S. Hao and Y. Li, *Solid State Sci.*, 2009, **11**, 2133.
30 V. G. Kessler, G. A. Seisenbaeva, M. Unell and S. Håkansson, *Angew. Chem., Int. Ed.*, 2008, **47**, 8506.
31 V. G. Kessler, G. I. Spijksma, G. A. Seisenbaeva, S. Håkansson., D. H. A. Blank and H. J. M. Bouwmeester, *J. Sol-Gel Sci. Technol.*, 2006, **40**, 163.
32 *Catalysis by ceria and related materials: Catalytic Science Series*, ed. A. Trovarelli, Imperial College Press, London, 2002.
33 J. Kašpar, P. Fornasiero and M. Graziani, *Catal. Today*, 1999, **50**, 285.
34 J. Kašpar, P. Fornasiero and M. Graziani, *Handb. Phys. Chem. Rare Earths*, 2000, **29**, 159.
35 B. C. H. Steele, *Nature*, 1999, **400**, 619.
36 B. C. H. Steele, *J. Mater. Sci.*, 2001, **36**, 1053.
37 B. C. H. Steele and A. Heinzel, *Nature*, 2001, **414**, 345.
38 R. X. Li, S. Yabe, M. Yamashita, S. Momose, S. Yoshida, S. Yin and T. Sato, *Solid State Ionics*, 2002, **151**, 235.
39 W. C. Maskell, *Solid State Ionics*, 2000, **134**, 43.
40 R. Ramamoorthy, P. K. Dutta and S. A. Akbar, *J. Mater. Sci.*, 2003, **38**, 4271.
41 J. Riegel, H. Neumann and H. M. Wiedenmann, *Solid State Ionics*, 2002, **152**, 783.
42 J. H. Lee, *J. Mater. Sci.*, 2003, **38**, 4247.
43 M. Cain and R. Morrell, *Appl. Organomet. Chem.*, 2001, **15**, 321.
44 Z. Hu, M. Xue, Q. Zhang, Q. Sheng and Y. Liu, *Dyes Pigm.*, 2008, **76**, 173.
45 E. Borgarello, J. Kiwi, M. Gratzel, E. Pelizzetti and M. Viscal, *J. Am. Chem. Soc.*, 1982, **104**, 2996.
46 M. Martos, B. Julián-López, J. V. Folgado, E. Cordoncillo and P. Escribano, *Eur. J. Inorg. Chem.*, 2008, 3163.
47 V. S. Vishnu, G. George and M. L. P. Reddy, *Dyes Pigm.*, 2010, **85**, 117.
48 G. Gauthier, S. Jobic, M. Evain, H.-J. Koo, M.-H. Whangbo, C. Fouassier and R. Brec, *Chem. Mater.*, 2003, **15**, 828.

